5

Laser welding application in crashworthiness parts

Nuno Peixinho
University of Minho – Dept. Mechanical Engineering
Portugal

1. Introduction

This chapter presents applications and research results of laser welding in crashworthiness parts. The term "structural crashworthiness" is used to describe an investigation into the impact performance of a structure when it collides with another object. This type of study is required in order to calculate the forces during a collision, which are needed to assess the damage of structures and the survivability of passengers in vehicles, for example. An important aspect of crashworthiness studies deals with impact energy absorption since the main purpose of vehicle crashworthiness is the dissipation of energy in specially designed zones while maintaining a survival space for passengers in stiff zones.
Several important technologies have been used to improve the crashworthiness of structures. Particularly in the transportation industry, the conflicting requirements of weight reduction, emissions reduction, improvement of energy absorption and reduction of intrusion and force levels, has led to advances in different areas: materials (increased use of light-alloys, polymers and high-strength steels), technologies (laser welding, tailor-welded blanks, hydroforming), design tools (computational power, advanced software, analytical tools).
The improvement of crashworthiness and reduction of weight using high strength steels (or other alternative materials) cannot be applied directly without considering other features. Thickness reduction cannot be performed without taking into account other design restrictions, particularly stiffness, but also dynamic stability i.e. resistance to the transition from progressive folding to global buckling. For this purpose design simulation tools such as the finite element method can make an important contribution. But also a conjugation with developments in technology processing can be adopted since laser welding and hydroforming have the potential to increase stiffness.
The interest of laser welding is related to the concept of intelligent design wherein the manufacturing process can bring advantages to both energy absorption and stiffness thereby increasing the potential advantage of using higher strength materials. Of particular importance has been the use of laser welding in tailor welded blank technology, which further allows the use of material in a more efficient way. For example, using higher thickness sheet metal where it is more needed. Or using higher strength materials in areas where more strength is needed. The application of such concept is currently in use but can become more widespread with more extensive research and driven by the need to reduce

weight in automobile structures. Joining of dissimilar materials has been given much attention in recent years due to their superior functional capabilities. The welding in tailor welded blanks of different high strength steels has already been accomplished and tested by the author. The application in beam structures of Dual-Phase DP600 and DP1000 steel materials with different thicknesses allowed for improvements in specific energy absorption in impact loading.

This chapter presents a literature review of the application of laser welding in crashworthiness parts, including a description of relevant background information, major issues, current trends and future challenges. Additionally several research results and applications from the author's experience are presented. These include:

- Laser welded crashworthiness parts: impact energy absorption of tubular structures and use of tailor welded blank technology in beam structures made of dissimilar materials (Figure 1);
- Application of laser welding in the development of components with localized thermal triggers.

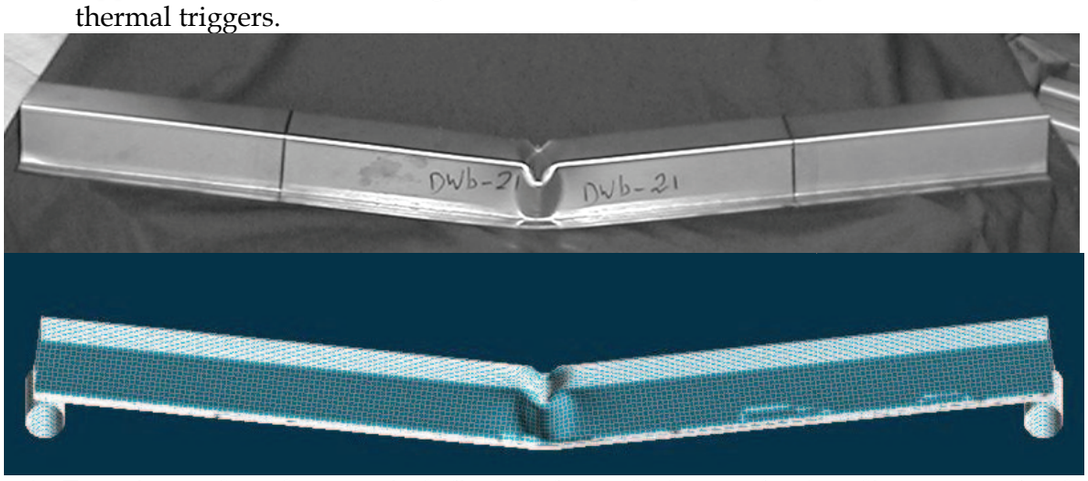

Fig. 1. Experimental and numerical final deformed shapes for bending tests of tubes manufactured using laser welding and tailored blanks (DP600 + DP800)

2. Laser Welding process and applications

For several years car body assembly techniques were dominated by spot-welding techniques. Resistance spot-welding is an affordable technology to join steel sheets and other metals. It can also be effectively automated while not requiring special preparation of the parts before joining. However, it has some disadvantages: spot connection system can cause high stress concentration near its location that can lead to local failure; there is a heat-affected zone and therefore a local modification in the material strength and relevant residual stresses; spot welding cannot be used to join different materials, unless using costlier special procedures. Laser-welding, as an alternative procedure, is a continuous joining technique, yet a very flexible process that can also be easily made automatic. Recent developments in high power CO2 lasers and robotic control have accelerated the application of laser-welding to vehicle structure fabrication and assembly in the automotive industry. It has also been shown that laser-welding gives many advantages if compared with other welding processes: a low heat input; a small heat-affected zone (Figure 2); low welding distortion, welding in an exact and reproducible manner, and welding at high speed. With

the introduction of new laser technology, such as high power Nd:YAG and CO2 lasers and fibre-optic beam delivery systems, the automotive industry is re-evaluating assembly systems for body manufacture.

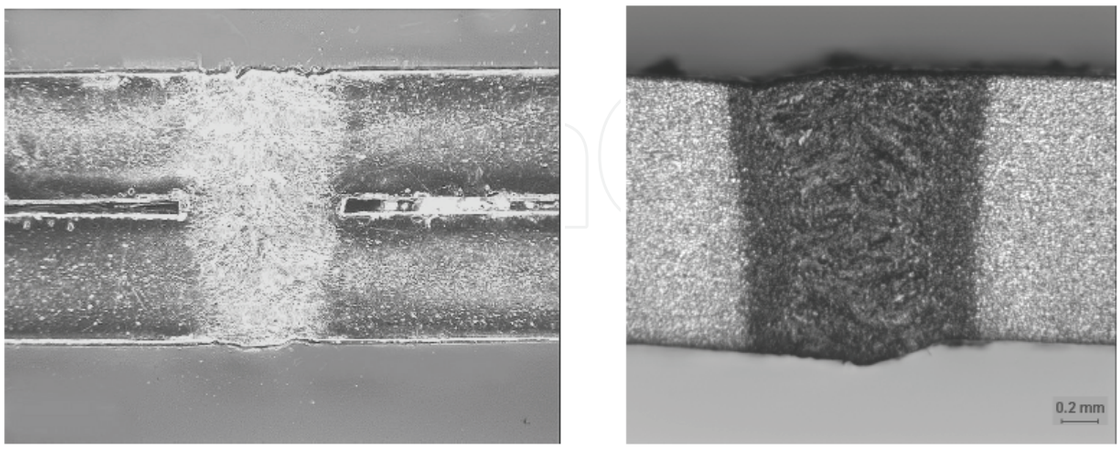

a) b)

Fig. 2. Examples of laser welds: a) lap weld; b) butt weld

Welding occurs when materials are heated to a molten state and fused together. Lasers generate light energy that can be absorbed into materials and converted to heat energy. By employing a light beam in the visible or infrared portion of the electromagnetic spectrum, energy can be transmitted from its source to the material using delivery optics which can focus and direct the energy to a very small, precise point. Since the laser emits coherent radiation, the beam of energy has minimal divergence and can travel large distances without significant loss of beam quality or energy.

Laser welding techniques take advantage of the capability for applying thermal energy to small areas in an efficient manner. This feature offers some distinctive metallurgical advantages in some welding applications, but also creates some unique problems. Since the surface heating generated by the laser light relies upon the material's heat conductivity to produce the weld, penetration is usually limited to less than 2 millimeters. However, using a technique known as "keyholing," higher power lasers (>106 W/cm²) can make deeper penetrations: by heating the spot of laser focus above the boiling point, a vaporized hole is formed in the metal. This is filled with ionized metallic gas and becomes an effective absorber, trapping about 95 percent of the laser energy into a cylindrical volume, known as a keyhole. Temperatures within this keyhole can reach as high as 25,000 °C, making the keyholing technique very efficient. Instead of heat being conducted mainly downward from the surface, it is conducted radially outward from the keyhole, forming a molten region surrounding the vapor. As the laser beam moves along the work-piece, the molten metal fills in behind the keyhole and solidifies to form the weld.

Generally, there are two types of lasers that are being used for welding operation: CO2 and Nd:YAG. Both CO2 and Nd:YAG lasers operate in the infrared region of the electromagnetic radiation spectrum, invisible to the human eye. The Nd:YAG provides its primary light output in the near-infrared, at a wavelength of 1.06 microns. This wavelength is well absorbed by conductive materials, with a typical reflectance of about 20 to 30 percent for most metals. The near-infrared radiation permits the use of standard optics to achieve

focused spot sizes as small as 0.025mm diameter. CO2 lasers have an output wavelength of 10.6 micron and an initial reflectance of about 80 percent to 90 percent for most metals thus requiring special optics to focus the beam to a minimum spot size of 0.08mm to 0.1mm diameter. However, whereas Nd:YAG lasers have power outputs up to 500 watts, CO2 systems can easily supply 10,000 watts and greater. As a result of these differences, the two laser types are usually employed for different applications. The powerful CO2 lasers overcome the high reflectance by keyholing, wherein the absorption approaches blackbody. The reflectivity of the metal is only important until the keyhole weld begins. Once the material's surface at the point of focus approaches its melting point, the reflectivity drops within microseconds.

One of the most promising technologies enabled by laser welding is tailor welded blanks. The application of such concept is becoming more widespread, driven by the need to reduce weight in automobile structures. Several challenges related to tailor welded blank technology have been addressed in recent years. Gaied and co-authors (Gaied et al., 2009) performed an experimental and numerical assessment of the formability of tailor welded blanks, being possible to predict the behavior of forming limit curves numerically and match with experimental results. Another recent study (Sheng, 2008) was focused on the forming of tailor welded strips with the interest of application in progressive forming. Dome tests were conducted and compared with simulation results allowing the validation of the approach for progressive forming. The forming parameters and processing dial-up for tailor welded blanks presents its own challenges (Panda & Kumar, 2001) as described in a study on the improvement of formability through application of counter pressure in biaxial stretch forming of tailor welded parts.

Joining of dissimilar materials has been given much attention in recent years due to their superior functional capabilities. The application in tailor welded blanks of different high strength steels has already been accomplished and tested by the author (Peixinho, 2004). The application in beam structures of Dual-Phase DP600 and DP1000 steel materials with different thicknesses allowed for improvements in specific energy absorption in impact loading. Another combination of dissimilar materials is of aluminium with steel due to its potential application in aerospace and automotive industries. Joining material combinations such as aluminium and steel poses a number of problems including formation of brittle intermetallic compounds, poor wetting behaviour of aluminium and differences in physical and chemical properties of the base metals. A recent numerical study by Padmanabhan and co-authors (Padmanabhan et al., 2008) determined the formability characteristics of aluminium–steel tailor-welded blanks. Aluminium (AA6016-T4) blank sheet was combined with a range of steel blank sheets namely, mild-steel (DC06) and high strength steels (AISI-1018, HSLA-340, and DP600) to form four different Al–steel tailor-welded models.

Other numerical studies on tailor welded blanks (Liu et al., 2007) and (Qiu & Chen, 2007), have clarified the need for reliable and numerical simulations in stamping and hydroforming processing of tailor welded blanks. The reliability of numerical simulations is a resultant of mesh quality, finite element formulation but also the availability of material properties that describe adequately material behaviour. For example, (Cheng et al., 2007) presented an experimental method of analysis to determine the tensile properties of welds of the heterogeneous tailor-welded blank (TWB) and its base metal. A real-time microscopic recording system was developed to acquire the true stress–strain data of the weld during tensile testing. A characterization of tensile properties of tailor welded IF steel sheets was

also presented by Panda and co-authors (Panda et al., 2007). Efficient numerical models can also be used for design optimization of welded blanks, as presented by (Kim et al., 2000).
The design of vehicle front structures for crashworthiness is commonly based on a series of rigid subsystems that constitute a nearly undeformable survival cell for the passengers, and deformable subsystems able to efficiently dissipate the vehicle kinetic energy. During frontal crash the front rails represent the main deformable components aimed to dissipate the kinetic energy of the vehicle, therefore their behaviour is crucial to obtain good vehicle performance, with stable and controlled energy dissipation. The design of the front rail, usually consisting of a thin-walled prismatic column, requires definition of materials and geometry: shape and dimensions of the cross section, thickness of the material.
An important issue in automotive design the trend for adopting materials allowing more efficiency. Widely used materials like deep-drawing steels are being substituted by high strength steels (dual-phase, TRIP steels.), aluminium alloys, magnesium alloys, and various types of polymeric materials and composites. There are several reasons for this change: the structure weight reduction that allows for more accessories and safety components, the need for higher stiffness and strength of the car body structure and cost reduction. Several problems are associated to the introduction of new materials: their properties are still not completely known, the usually adopted technologies are sometimes not usable anymore, and new environmental and protection problems arise. Additional problems are associated to the joining techniques.
Regarding laser-welded tubular structures subjected to impact loading there are not extensive results available in the literature. Radlmayr and co-authors (Radlmayr et al., 1993) examined octagonal sections, whereas (Geoffroy et al., 1993) reported that laser-welded crash boxes have slightly improved or similar energy absorption characteristics, as compared to spot-welded ones, but a consistent stabilization effect of the plastic folding was obtained. The author (Peixinho et al., 2006) presented experimental and numerical results for impact testing of thin-walled structures made of high strength steels and using spot-welding, laser welding and tailor welded blanks techniques. The results highlighted the advantages of continuous joints in thin-walled structures and improvements in energy absorption using laser welding and tailor welded blank technology. Peroni and co authors (Peroni et al., 2009) presented results of an experimental program aimed to study the progressive collapse behaviour of some thin-walled closed-section structural sections made from deep-drawing steels and joined with different joining. Solutions characterized by different continuous joining technologies were examined and compared to the usual spot-welding solution. The obtained results indicate that continuously joined structures are at least equivalent to and generally better than spot-welded structures, and have further advantages typical of these joining solutions (higher stiffness and fatigue strength, improved vibration response, especially in the case of adhesive joints). Stability of folding was reported as much improved with laser welding compared to the other joining solutions.

3. Research work in laser welding applications

3.1 Laser welded crashworthiness parts

This section presents results from an experimental program that included quasi-static and dynamic testing of tubes made of high-strength steels, as described in (Peixinho, 2004). These included short tubes, with a length of 250 mm for axial crush testing, and tubes with a

length of 1000 mm used in three-point bending tests. The selection of the geometries was motivated by practical loading situations and structural sections commonly used in crash-absorbing structures and components. This was the case with the top-hat sections. Also the hexagonal section was examined since it should be more efficient than the traditional top-hat and double-hat sections.

The materials examined are Dual-Phase and TRIP steels, having commercial designations: DP600; DP800; TRIP600. These designations reflect the nominal Ultimate Tensile Strength of the material. All investigated steels were industrially melted, cold-rolled, annealed and temper rolled to a final thickness between 1.0 and 1.4 mm. They were tested in the as-shipped condition. Table 1 shows the nominal chemical compositions of the investigated steels, the elements not mentioned are within the usual limits for cold rolled steels. The chemical composition was obtained recurring to mass spectrometers: Philips model X'Unique II and Spectrolab model M5. Typical microstructures of the tested steels are shown in figures 3 and 4, obtained by optical microscopy and Scanning Electron Microscopy.

Steel grade	C (%)	Si (%)	Mn (%)	P (%)	S (%)	Nb (%)	Al (%)
DP600	0.11	0.31	0.78	0.015	0.01	-	0.04
DP800	0.13	0.21	1.48	0.015	0.01	0.02	0.04
TRIP600	0.23	0.33	1.49	0.011	-	-	0.88

Table 1. Nominal chemical composition, mass contents in %

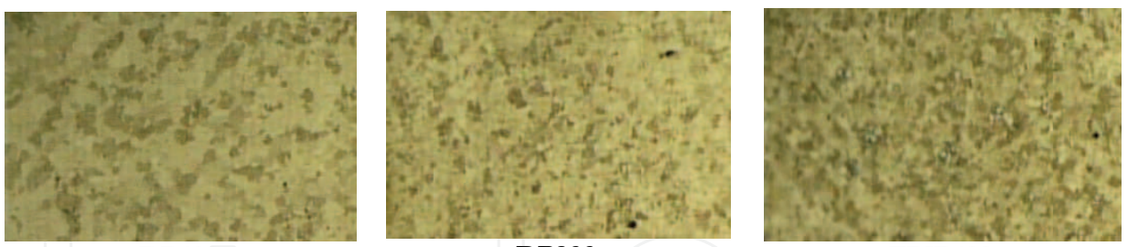

DP600 DP800 TRIP600

Fig. 3. Optical micrographs of steel samples (200x)

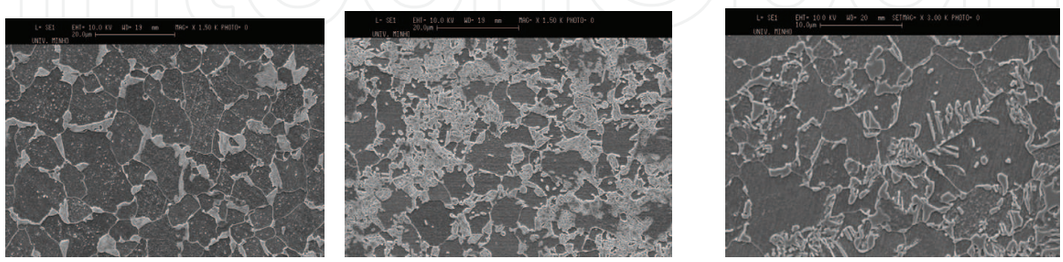

DP600 DP800 TRIP600

Fig. 4. SEM images of microstructures (1500x)

Besides the three types of steels, top-hat and hexagonal geometries, also spot welding and laser welding technologies were used in the manufacturing of tubes. Laser welds were performed continuously at the centre of the joining flanges of the tubes. After specimens had been cut to length, the end faces were ground to ensure the faces were square and parallel to each other. Generally the tubes used for dynamic testing were manufactured with triggers. These are indentations in the tubes used to initiate the folding process. The crush and bend tests were performed using three different test equipments to cater for different test speeds. A summary of the experimental program is shown in table 2. In figure 5 the nominal dimensions of the studied sections are presented.
The bending tests were performed on tubes with a top-hat geometry and having dimensions of the section presented in figure 5.a). Some of these tubes were manufactured using two different steel grades: DP600 and DP800 with the manufacturing process making use of tailor welded blank construction. In this case, the central section of the tubes was manufactured with DP800 and the extremities using DP600. This type of solution is currently of great interest for the automotive industry since it allows the manufacture of components having a variable thickness. In this way greater weight efficiency can be achieved since higher thickness can be used in specific locations, for example in the impacted area of a energy-absorbing beam. In this case case, besides different thickness, also different materials were used which makes the welding process more difficult. The set-up for the bending tests is presented in figure 6. The details of the tubes manufactured using tailor-welded blanks are presented in figure 7.

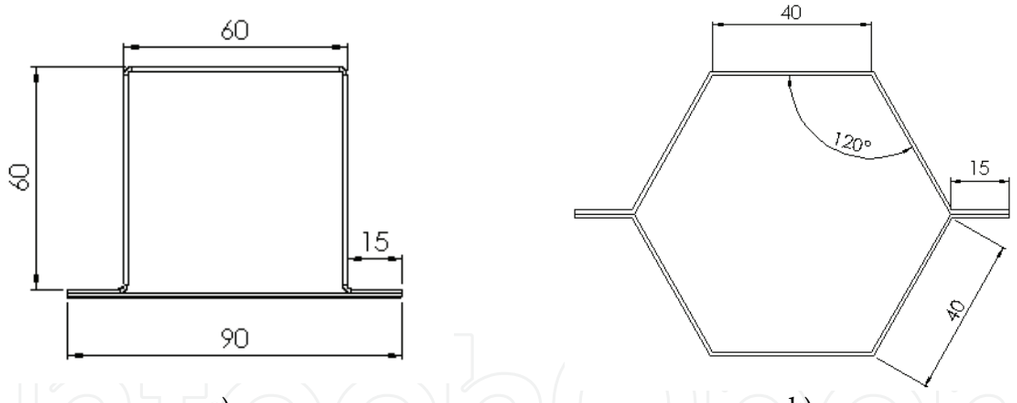

a) b)

Fig. 5. Nominal dimensions of sections: a) Top-hat; b) Hexagonal

Material	Geometry		Welding technique		Trigger	Reference of tests
	Top-hat	Hexagonal	Laser	Spot-weld		
Axial Crush tests						
DP600	V		V		V	DW1; DW2; DW3; DW4 Dtc7; dtc8
	V		V			DW17 QS4; QS5; QS6
	V			V		DW5; DW6; DW7; DW8 dtc3; dtc4 QS1; QS2; QS3

TRIP600	V		V		V	DW9; DW10; DW11; DW12 dtc1; dtc2
	V		V(1)		V	DW22; DW23 QS13; QS14
		V	V		V	DW13; DW14; DW15; DW16 dtc5; dtc6
	V		V			DW18 QS7; QS8; QS9
		V	V			QS10; QS11; QS12
	V			V		DW24; DW25; DW25; DW27 QS15; QS16
Bending tests						
DP800	V		V			DWb19; DWb20 QSb1; QSb2
DP800+DP600	V		V(2)			DWb21 QSb3; QSb4

(1) Laser-welding using two parallel welds
(2) Tube manufacturing using tailor-welded blanks

Legend of test nomenclature:
DW: drop-weight crush tests
DWb: drop-weight bending tests
dtc: crush tests at 250 mm/s
dtcb: bending tests at 250 mm/s
QS: quasi-static crush tests
QSb: quasi-static bending tests

Table 2. Summary of experimental program

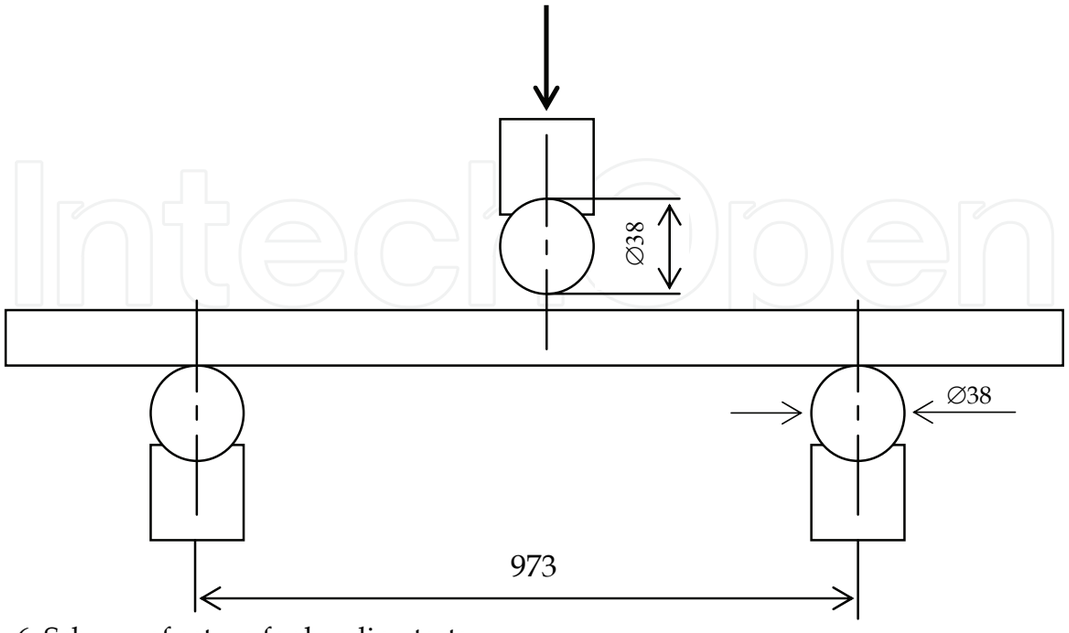

Fig. 6. Schema of set-up for bending tests

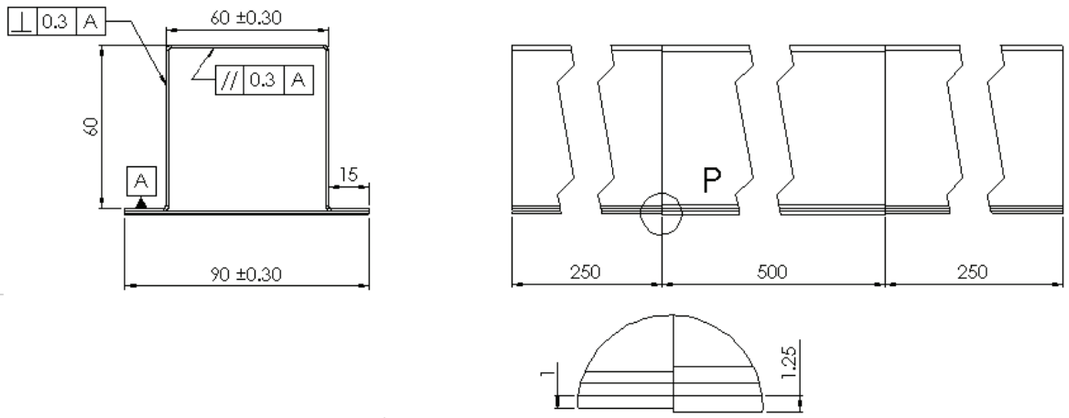

a)

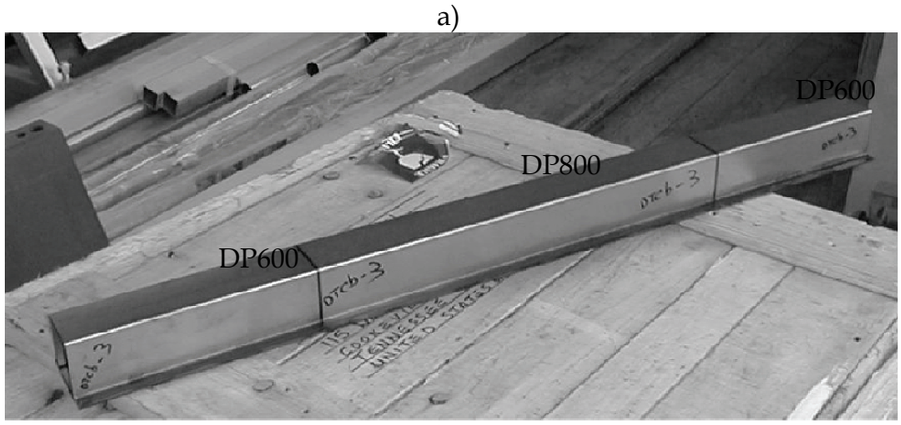

b)

Fig. 7. a), b). Details of tubes manufactured using tailor welded blanks

Quasi-static tests on thin-walled tubes were performed on a DARTEC M1000 machine with a 600kN capacity. The DARTEC machine was operated at a constant cross-head speed of 0.1 mm/s. During the tests, the compressive load and displacement were measured using a strain-gauge load-cell and a LVDT. The machine was controlled by a PC that also recorded and processed the measured data from the test machine. The entire crushing process was composed of individual strokes of 90 mm displacement, as the test machine was only capable of performing strokes to a maximum of 100 mm extension. The bending tests were performed with only one stroke of 90 mm displacement.

Several tests were performed at intermediate speeds of approximately 250 mm/s, using a DARTEC testing machine with a load capacity of 250kN. The control of the test machine and recording of data also made use of a PC. In this equipment the specimens were placed centrally and upright between two endplates but without any further support.

The impact tests were conducted on a drop hammer. The crush tubes were impacted at their top by a falling mass, which was laterally guided by rails. The specimens were placed vertically on an anvil and hit by the impactor. No end constraints were provided, however special care was taken with the surfaces of the anvil, impactor and test specimens in order to obtain parallel faces. This included machining the top ends of the tubes as well as the anvil and the impacting face of the falling mass. The impactor used in the dynamic bending tests

had a cylindrical end with a 38mm diameter and a support for the tubes as presented in figure 6.
The dynamic tests were carried out at test energies ranging from 0.575 to 14.270 kJ. Different test energies were obtained changing the drop height and the impact mass. Figure 8 shows the drop hammer rig as well as associated instrumentation, test supports and specimens. A Laser-Doppler velocimeter was used to obtain the velocity-time history during the dynamic tests. It was then possible to obtain the load-time, displacement-time and load-displacement histories. From these data, the axial displacement, or crushing distance, as well as the displacement averaged mean load values may be calculated.

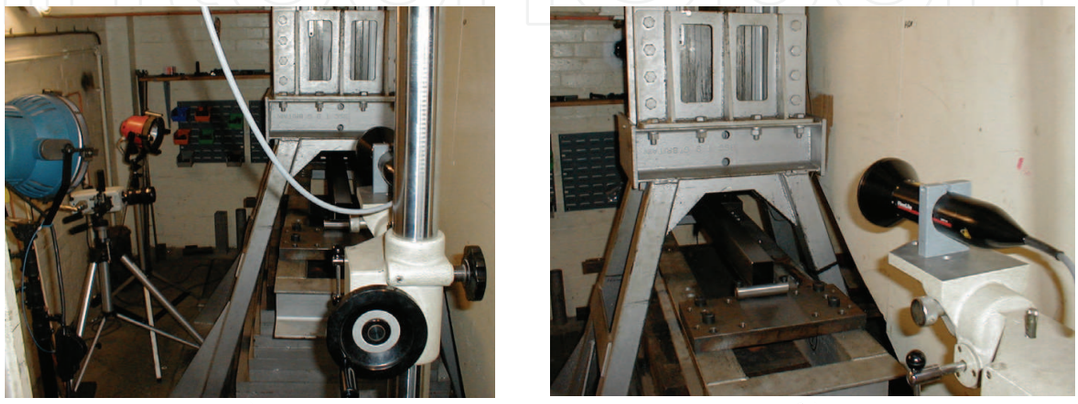

a) b)

Fig. 8. a) Drop-hammer rig and instrumentation (recording camera on the left); b) Image of drop-hammer rig with Laser-Doppler velocimeter in the foreground.

The crushing tests of tubes were used to determine of maximum crushing force $P_{máx}$, mean crushing force P_m, absorbed energy E_a, as well as to perform a qualitative analysis of the crushing behaviour that included the number of lobes formed, types of lobes, and collapse type. The specimens were accurately measured prior to and after testing. The total crushing distance δ was measured as the difference of the height of the specimen before and after testing. The recorded force-displacement curves obtained in the DARTEC tests were integrated with respect to the deflection δ to determine the mean crushing force. The mean load P_m was then calculated using the expression:

$$P_m = \frac{E_a}{\delta_f} \tag{1}$$

where δ_f is the final deflection. The mean load is an indication of the energy-absorbing ability of a structure, when compared to the axial displacement required to absorb that energy. Subsequently, the mean load and absorbed energy were also calculated for prescribed displacement values. The maximum crushing force was determined from the load curves. However, this value is only reliably obtained in the quasi-static tests since inertia effects and fluctuations in the initial load peak exist in the dynamic tests which makes accurate recording difficult.

In the dynamic tests the velocity-time readings obtained with the Laser-Doppler velocimeter were differentiated and integrated to obtain the load-time, displacement-time and load-displacement histories. From these data, the axial displacement, or crushing distance, as well as the displacement averaged mean load values may be calculated using the absorbed energy in the same manner as with the quasi-static tests.
In general, the spot-welds resisted well the loading and deformations. Besides localised material fracture, only in a few tubes and in a few locations, spot-welds were halfway torn apart. Laser welds only presented problems for the TRIP600 steel. Only in a few of the top-hat tubes manufactured with this material it was possible to obtain regular progressive folding without separation of the hat-section and closeout panel. However, the hexagonal laser-welded sections and the spot-welded tubes manufactured with TRIP600 did not present that problem.
The analysis of results of energy absorption properties should consider the folding behaviour and its initiation. Generally, the dynamic tube crushing tests made use of initiators or triggers in the form of indentations in the tubes. These worked satisfactorily in the dynamic tests, providing an efficient initialisation of the crushing process near the top of the specimen (proximal face to the impact mass). This feature could be observed from the camera recordings. Figures 9 and 10 present examples of the initiation of folding. The images were obtained with the recording camera rotated for best resolution within the test area.

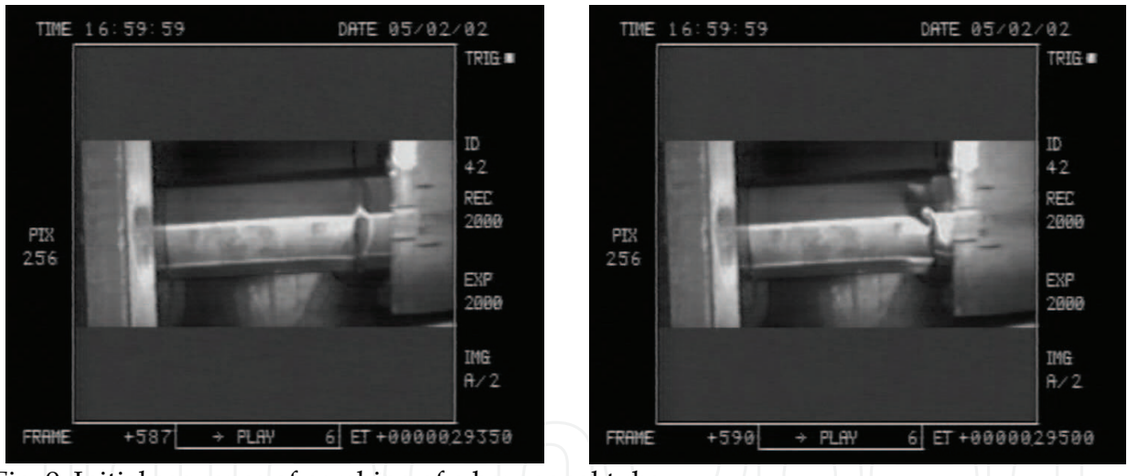

Fig. 9. Initial sequence of crushing of a hexagonal tube

Generally, buckling was initiated at the proximal face of the specimens and progressed towards the distal end. However, in some cases, there was a simultaneous initiation of folding at both ends with a plastic buckle being developed near the distal end of the specimen. This buckle generally remained stable during further deformation of the specimen, which could be attributed to the contribution of the triggers at the opposite end of the specimens. In some of the tests with spot-welded tubes this buckle caused a near-simultaneous progression of the crushing process from both ends, or also instability towards the end of the deformation process. Since the spot-welded tube did not have triggers this occurrence is attributed to the competition between both ends in the contribution to the deformation process. In figure 10 this occurrence is also observed.

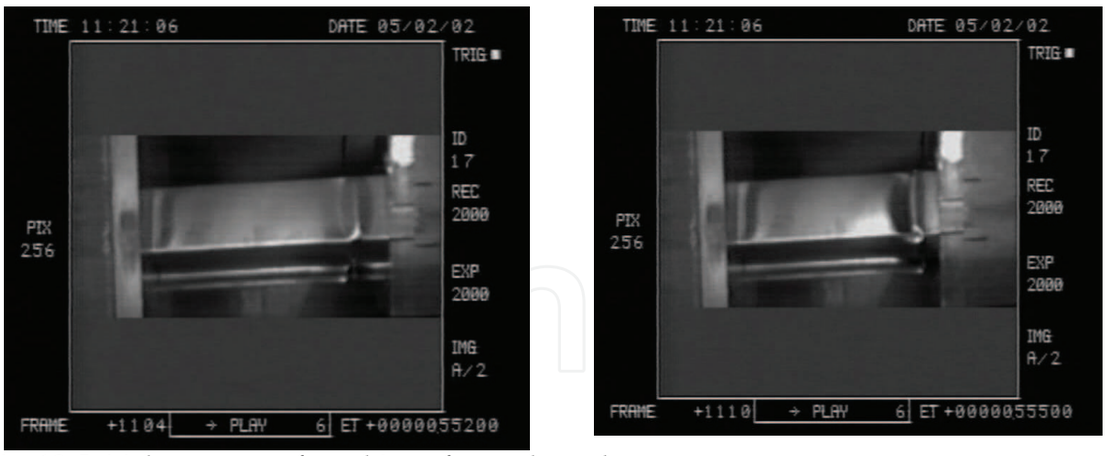

Fig. 10. Initial sequence of crushing of a top-hat tube

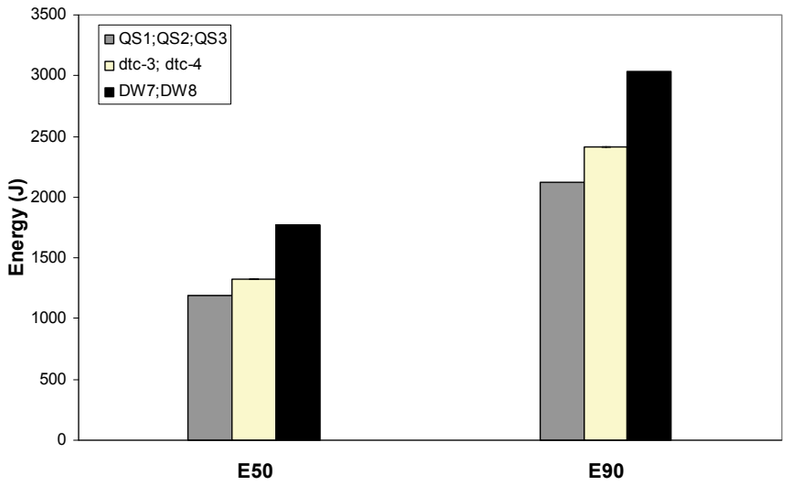

Fig. 11. Absorbed energies for DP600, top-hat geometry, spot welding

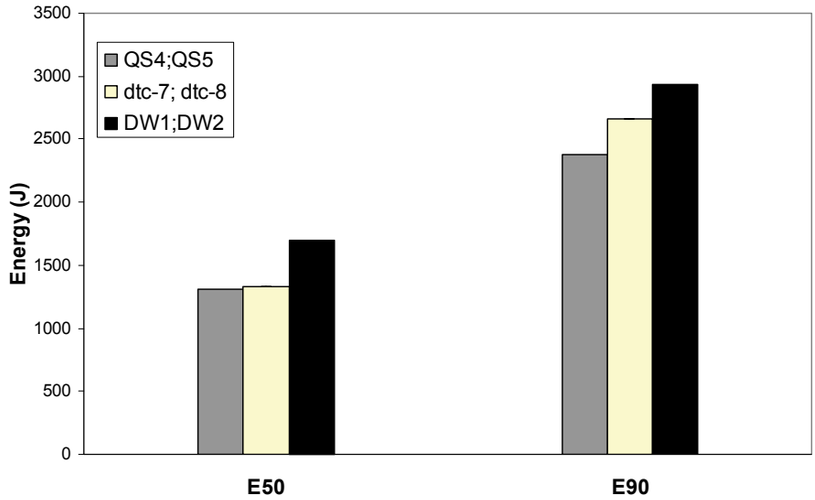

Fig. 12. Absorbed energies for DP600, top-hat geometry, laser welding

Several features can be observed from the results that allow a comparison of different materials, geometries and welding processes. This analysis can be performed by comparing the absorbed energies at prescribed displacements, in this case energies at 50mm and 90mm of crushing length. This analysis is important since the absorption of energy and its management are critical to obtain crashworthy structures. In figures 11 to 13 examples of absorbed energies at different crushing lengths (E_{50}; E_{90}) and different test velocities are presented. In these cases an increase of absorbed energies for impact loading is observed which was expected when considering inertia and strain rate effects.

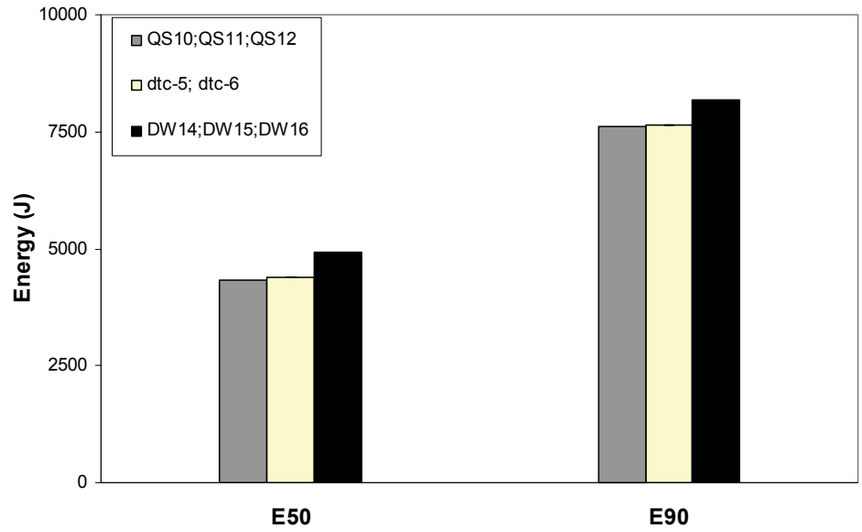

Fig. 13. Absorbed energies for TRIP600, hexagonal geometry, laser welding

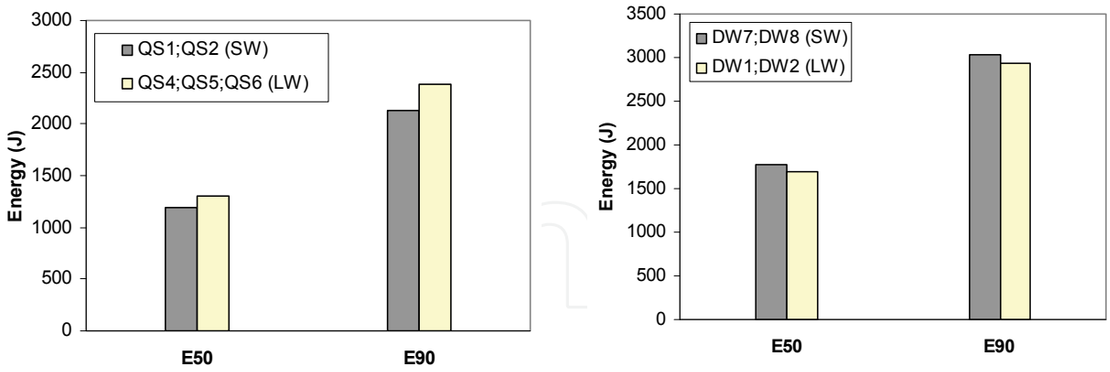

a) quasi-static crush tests b) dynamic crush tests

Fig. 14. Comparison of absorbed energies for spot-welded (SW) and laser welded(LW) top-hat tubes (DP600)

One of the observed characteristics in this study was the differences between spot-welded and laser welded connections used in the manufacturing process of the tubes. Figures 14 and 15 present a graphical comparison of absorbed energies in tubes manufactured using the two processes. The moderate increase in the amount of absorbed energy for a given

crush distance in laser welded connections was expected, considering previously published results. However, in figure 14-b) it is observed that at higher impact speeds the spot-welded tubes absorbed a higher amount of energy. This was not observed for TRIP600 steel, although with this material the difference in absorbed energies between spot-welded and laser welded tubes in dynamic crush testing was very small. It is possible that at impact loading the continuous connection obtained using laser welds has undergone some local separation although this was not observed in the tests considered for this analysis.

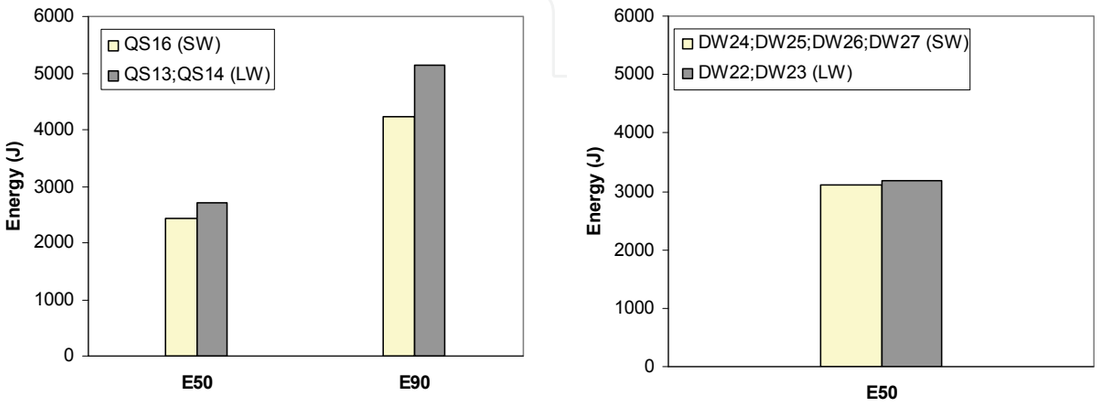

a) quasi-static crush tests b) dynamic crush tests

Fig. 15. Comparison of absorbed energies for spot-welded (SW) and laser welded (LW) top-hat tubes (TRIP600)

Another observed feature in the experimental tests was the efficiency of different sections for the purpose of energy absorption. This was possible in the tests of the TRIP600 material where the specific absorbed energies of top-hat and hexagonal sections were compared. Figure 16 presents results of that comparison. A remarkable increase in absorbed energy per unit weight is observed for hexagonal sections. This was expected considering existing results in the available literature (Auto/Steel Partnership, 1998) where the difference in the average static crush force between top-hat and hexagonal tubes having the same mass was of approximately 40%. In the present tests the increase in the average static crush force was of approximately 32% with the increase in the absorbed energies E_{50} and E_{90} ranging from 32.9 to 37.4 % in the quasi-static tests and 29.6 to 35.5% in the dynamic tests. This increase in the efficiency of the energy absorption is expected considering that thin-walled cylindrical shells have more efficient folding modes and that octagonal and hexagonal thin-walled sections are closer to the more efficient circular shape than top-hat sections.

In figure 17 a comparison of specific absorbed energies of DP600 and TRIP600 is presented, based in tests using the same geometry (top-hat). A noticeable increase in specific absorbed energy is observed for the TRIP600 material, in both quasi-static and dynamic tests. This difference can be attributed to the higher strain hardening and strength properties and also the higher elongation to fracture that implies a higher area under the stress-strain curve, which is directly related with energy absorption. However, it should be noted that the tests were performed in tubes manufactured using steel sheets with different thicknesses, which might induce differences in the folding process with consequences in the absorbed energy.

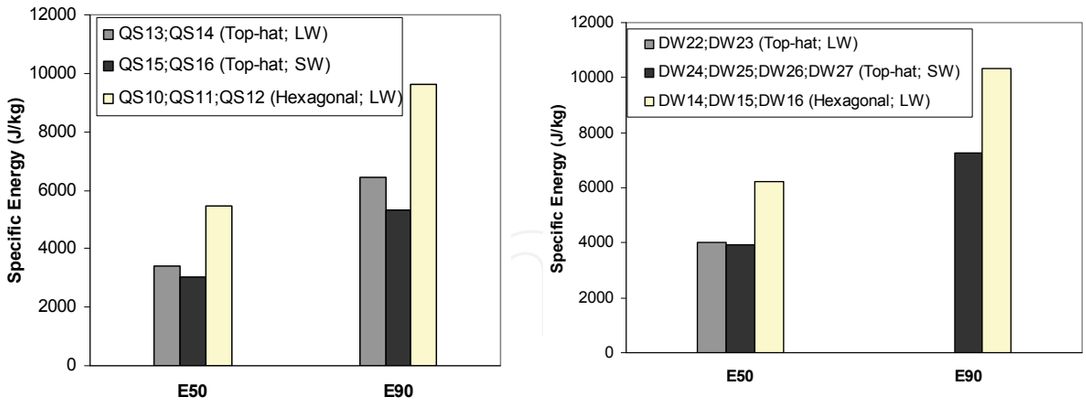

a) quasi-static crush tests b) dynamic crush tests

Fig. 16. Comparison of specific absorbed energies for top-hat and hexagonal tubes (TRIP600)

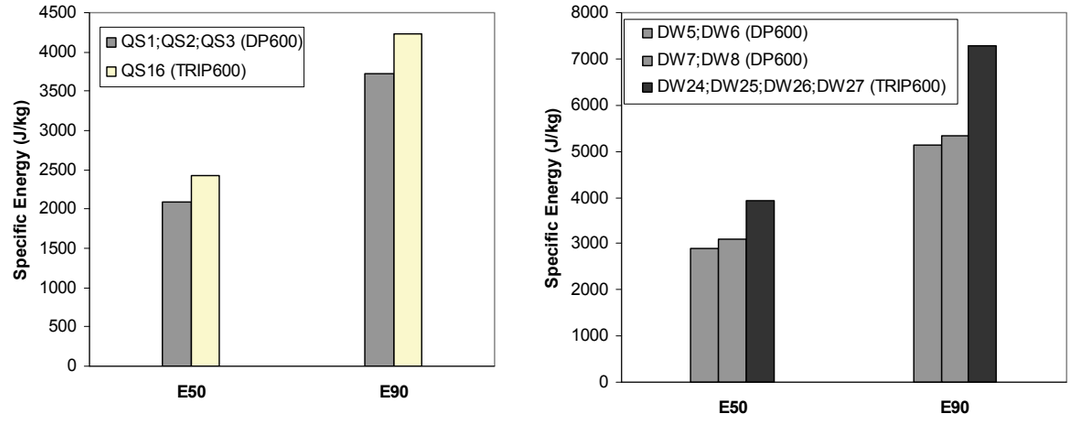

a) quasi-static crush tests b) dynamic crush tests

Fig. 17. Comparison of specific absorbed energies for DP600 and TRIP600 steels using top-hat geometry

The available data for bending tests allows the evaluation of some features. In figure 18 a comparison of quasi-static and dynamic absorbed energies is presented for the tubes manufactured using tailor-welded blanks. As expected a slight increase is observed for the dynamic case. Figure 19 presents a comparison of specific absorbed energies (E_{50} and total absorbed energy) between the tubes made of DP800 steel and the ones manufactured using tailor welded blanks (that use DP600 and DP800 steel grades). The tubes manufactured using tailor-welded blanks are more efficient because the plastic deformation is localized in the central area where the striker impacts the tube.

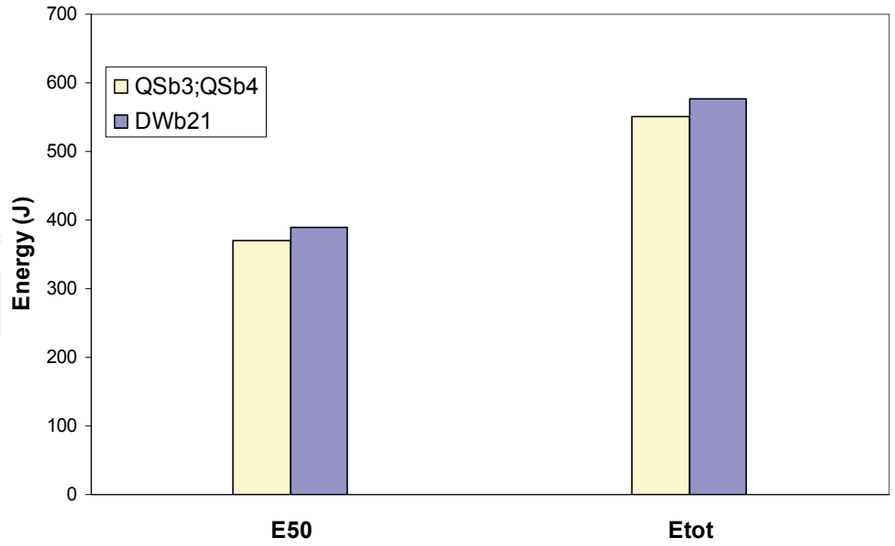

Fig. 18. Comparison of absorbed energies for bending tests of tailor welded tubes tested quasi-statically and dynamically.

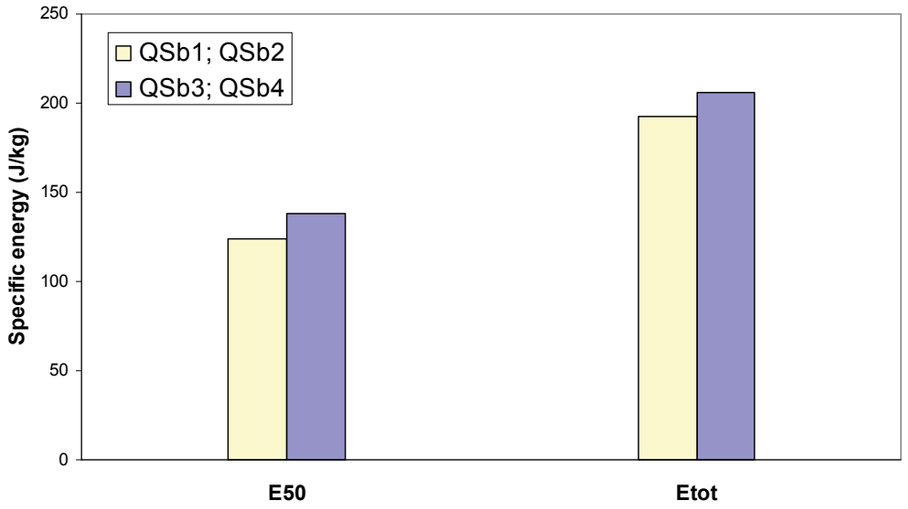

Fig. 19. Comparison of specific absorbed energies in bending tests of tubes manufactured using DP800 steel and tailor-welded blanks (DP600 and DP800 steel).

3.2 Application of laser welding in the development of components with localized thermal triggers

This section presents results of a study aimed at developing an approach consisting of local heating of aluminium alloy structures with the purpose of introducing a local modification of material properties. The main objective of this approach is the management of crash-energy absorption in a cost effective manner through the introduction of triggers: by local heating in areas chosen for triggers, local softening of aluminium can be induced thus

forcing the tubular structure to initiate deformation in prescribed locations and assure deformation in the mode of highest energy absorption.
Research studies have reported attempts to improve energy absorption of extruded aluminium tubing by artificially introducing various types of triggering dents (Kim, 2002); (Lee et al., 1999). The absorbed energy and crushing morphology were analyzed depending on number, shape, and location of triggering dents by using computer simulation.
The concept of using thermal modification of an aluminium alloy in localized areas can provide for a larger global deformation of a part and higher energy absorption before failure. Thus fracture in critical regions can be delayed and the total energy absorption can be accordingly increased. Such design features are also highly cost-effective in implementation compared to the alternative process of geometric redesign. This advantageous use of aluminium is therefore possible by applying "local material design", which in the present context is defined as controlled manipulation of material properties like strength, work hardening and ductility by means of non-homogenous heating, as originally presented (Bjørneklett & Myhr, 2003).
In particular, the buckling of crash boxes during a crash situation may be controlled by deliberately imposing local soft zones (i.e. thermally induced triggers). For the impact event simulation tools can be used to assess crashworthiness performance and even enable a combined simulation of the thermal processing and subsequent response in the final component subjected to dynamic loading.
This study presents preliminary results of temperature and heating cycle influence in material properties and microstructure of a selected 6060-T5 aluminium alloy. The objective of this research work is to improve the crushing stability and the absorption of energy originated from impact in tubular components. The improvement of the deformation is done by CO2 laser welding technology applied as a local heat treatment. This process will induce a micro structural modification caused by the heating in predefined zones that act as triggers of the folding process in the progressive impact energy absorption of tubular structures. It is well known that the 6060-T5 aluminum alloy suffers modifications in microstructure with heat-treatment. Technical literature presents different diagrams that show the behavior of this material at different temperatures and heat-cycle duration. It is shown that with temperature between 250 º C and 550 º C there is a significant modification in the microstructure with decrease on hardness. It should be mentioned that the time is also an important factor being the temperature and time interdependent

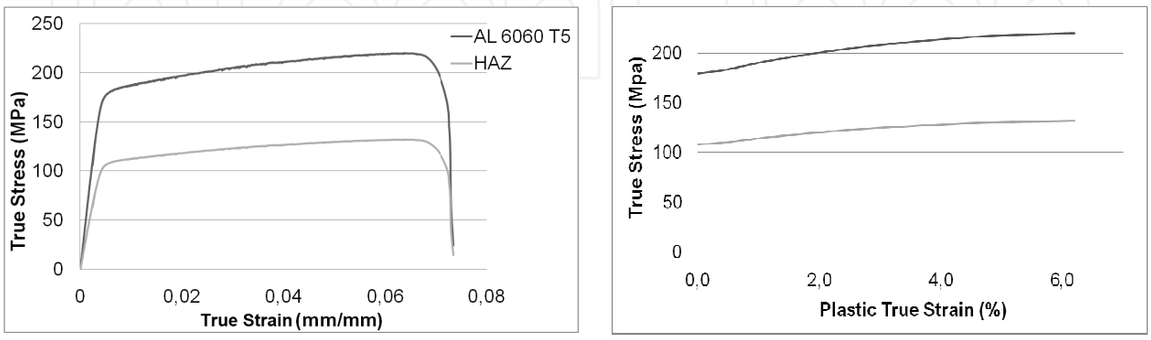

a) b)

Fig. 20 – a) AA 6060 T5 True stress–strain curve and on the heat affected zone; b) Model of plastic behaviour used in the numerical simulations.

The mechanical properties of the aluminium alloy 6060-T5 were obtained by static tensile tests, and the properties of the heating affected zone (HAZ) are about 60% less than the base material, according to the Vickers micro-hardness test, as one can see in Figure 20.
The aluminium alloy studied suffers modifications in microstructure for certain parameters, such as temperature and heating cycle. The significant changes in the microstructure of the alloy occur for temperatures between 250ºC and 550º C where a decrease in hardness occurs. This is attributed to the dissolution of copper rich precipitates due to the imposed thermal cycle. Appropriate choice of heating cycle parameters is also important because the alloy may not need very long temperature cycles for full transformation, or very high temperatures, and these two factors vary depending on another, being at this moment the objective of the heat treatment the highest softening possible of the alloy.
For carrying out the furnace heat treatment, several samples were cut from aluminium alloy sheet (average thickness 1.5mm). The cut samples were then subjected to heat treatment: each sample placed in the central zone of a furnace for prescribed temperature and time.
For the laser heat treatment a CO_2 laser welding machine was used (Trumpf – 4000W). This was found suitable for the local softening approach. The density of energy could be regulated from laser power and feed rate thus varying material parameters and the heat affected zone.

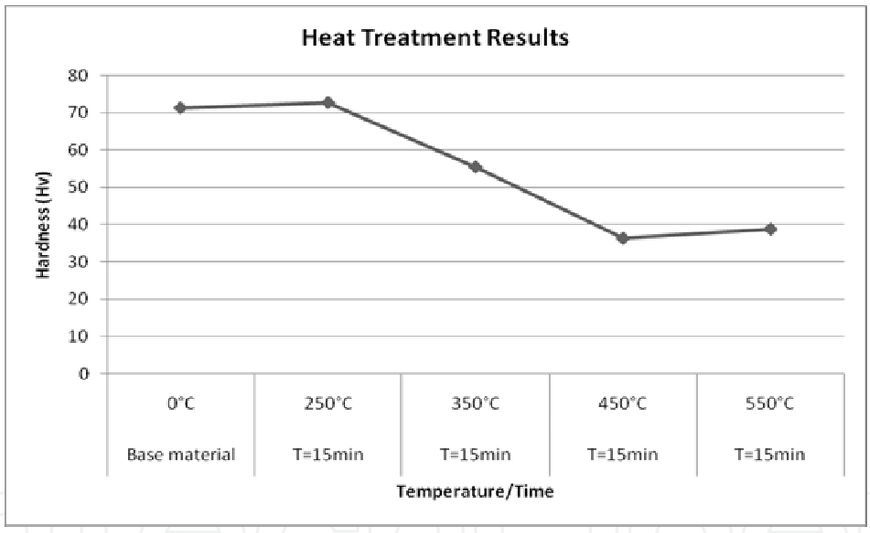

Fig. 21. Hardness results for furnace heat treatment.

Figure 21 presents results of Vickers micro-hardness test (with 100gf load) for the samples with furnace heat-treatment. Temperature and time are presented for the furnace tests.
The laser was used with 4 kW power and different feed rates. The hardness results and sample superficial aspect, presented in Figures 22 and 23, show a significant increase of the HAZ with the feed rate of 5 m/min. It is also possible to see that the minimum hardness, in the HAZ, is similar with the obtained in the bulk treated specimens (furnace heat treatment).

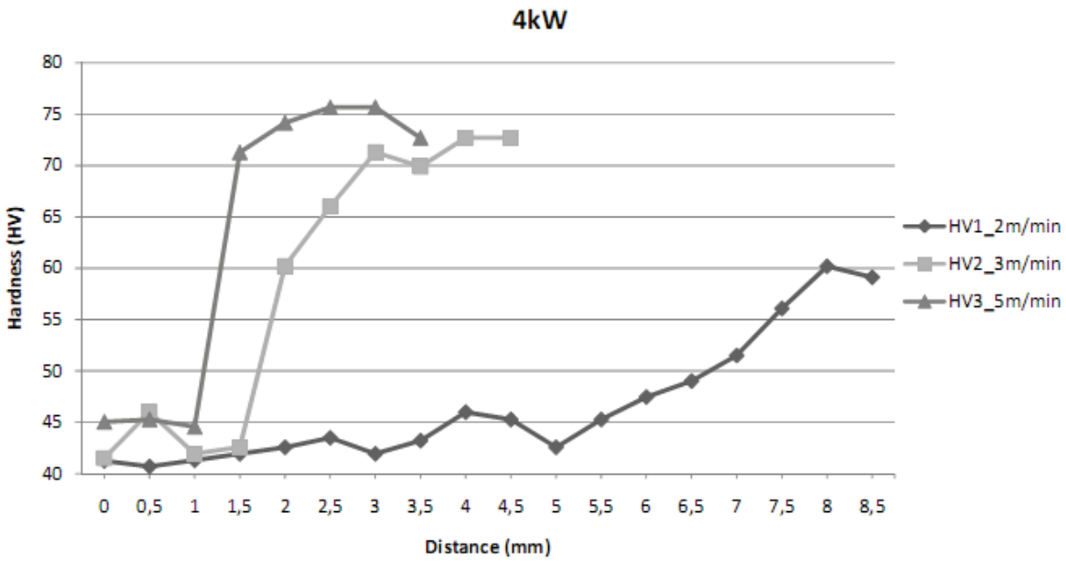

Fig. 22. Hardness results for laser heat treatment at center of HAZ (0 mm) and distance from center of HAZ.

4kW		
HV1_2m/min	**HV2_3m/min**	**HV3_5m/min**
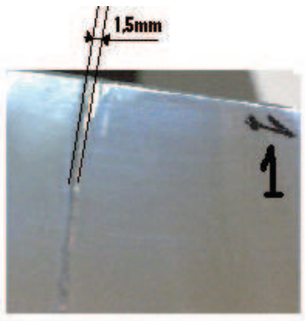		

Fig. 23. Images of the heat affected zone HAZ in samples treated with different laser speeds.

The structure considered in this study is a prismatic column with square cross-section of aluminium 6060-T5. The dimension of the cross-section is 75x75 mm with 1.5 mm wall thickness, and the length of the column is 300mm. The local heating in areas chosen for triggers will be modelled in the numerical simulations through the modification of the mechanical properties, as shown in figure 20.b). The location of these triggers on aluminium alloy will be precisely induced thus forcing the column to deform in that zone.

The mechanical properties considered on the numerical simulations are Young's modulus E=69×10³ MPa, Poisson's ratio ν=0.3, density ρ=2700Kg/m³ and the initial yield stress σ_y=180MPa for the base material and σ_y=108MPa for the heat affected zone (HAZ). The complete true stress–strain relation used in the simulations is shown in 20-b). As the aluminium is insensitive to the strain rate effect, this is neglected in the finite element modelling.

The present simulations were performed with the commercial software LS-DYNA that is appropriate for non-linear explicit dynamic simulation for large deformations. The loading condition is the impact of a rigid mass of 70kg at an initial speed of 45km/h on the top of the model, as shown in Figure 24.a), being the lower part of the model clamped.
The elements used in this type of modelling need a good bending capacity and membrane behaviour for large in-plane deformations allowing for axial loads. With these requirements the chosen element is a Belytschko-Lin-Tsay shell element of four nodes, which is commonly used in crash simulations. This element type is suitable for the large deformations which occur in the folding process. Five integration points were used in the thickness direction.

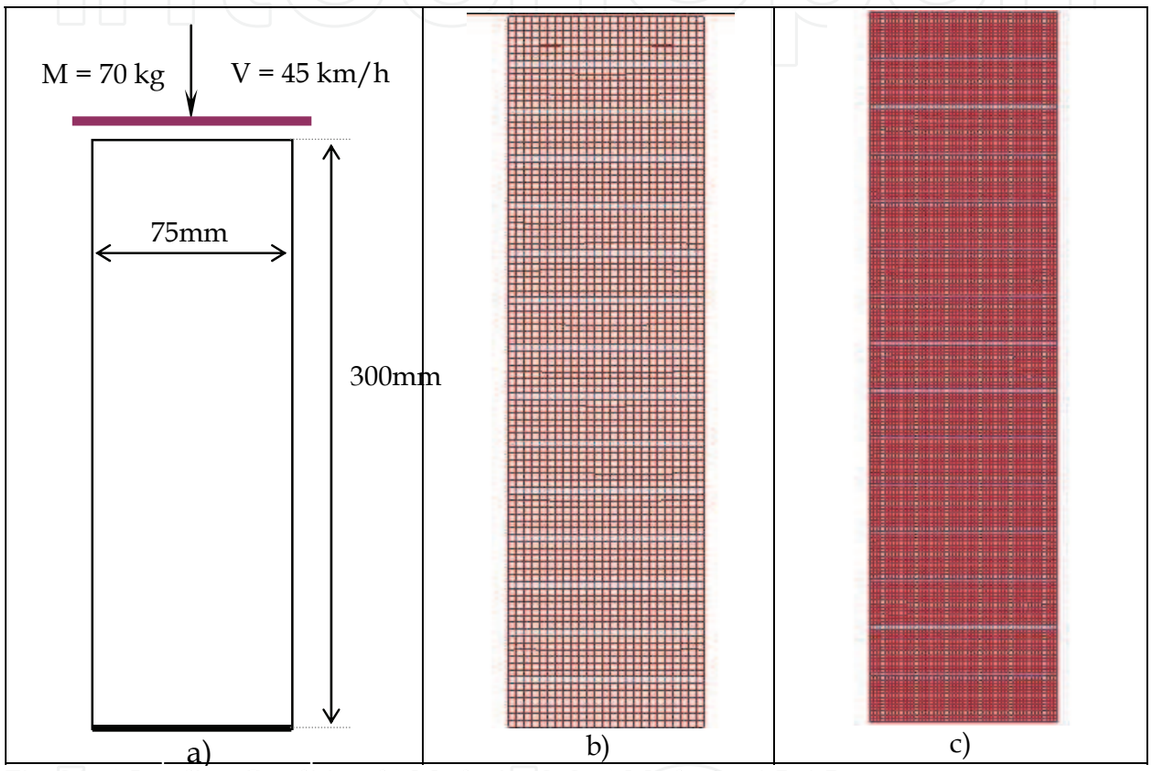

Fig. 24. a) Loading Condition; b) Mesh size 3x3; c) Mesh size 1.5x1.5

The contact between the rigid wall and the model is defined as surface-surface interaction with a friction coefficient equal to 0.1. Besides, self-contact with a friction coefficient 0.1 is defined on the model walls and gravitational acceleration is applied to the whole model.
In the numerical simulations the focus of the laser heat treatment was chosen for trigger dimension, and appropriate mesh size triggers are also chosen, as shown in Figure 24 b) and c). The studies are based on the 3mm and 1.5mm width of the laser focus, that is, the weld3 and weld1.5 as indicated in the figures.
A total of six triggered configurations were defined, depending on number, width, and location. The number of triggers can be largely divided into three types, i.e. without trigger, triggers in opposite sides (2 sides) and triggers around of the model (4 sides of the model), and their width is also varied either 3 or 1.5 mm, as shown in Table 3.
In all models the triggers are referenced to the top of the numerical model. For example, in reference 14x20 it is meant that the triggers are inserted in up to intervals of 20 mm, fourteen

triggers in along of the model. When the reference is 9x30 and 6x40 the same process is done, inserted at even intervals of 30mm/40mm with nine/six triggers in along of the model, respectively. For models with the reference 4x20, 4x30 and 4x40, only the initial four triggers are introduced in up to intervals of 20mm, 30mm and 40mm, respectively.
Plastic folds are initially formed in the upper part of the smart models, and continue to develop gradually down into the lower parts. Besides, as soon as the folds consist in a side of the model, they develop in the side opposed in turns. These folds are facilitating a mechanism to absorb the energy on the compressive deformation, therefore the tendency of formation of folds fulfils an important role in the absorption of energy.
The numerical results of some smart models are shown in Figures 25-27, where it is possible to observe that under dynamic loading models generally had a regular progressive folding, but some of them exhibited irregular plastic folding during the terminal crushing stages, as observed in model Weld3 4sides 4x20 (Figure 27), where the folds are well induced at the trigger sites in the initial phase of deformation, but showing quite unstable deformation later on. In both models without triggers, in the middle of the plastic deformation phase the folds are quite irregular inducing to a structural instability.

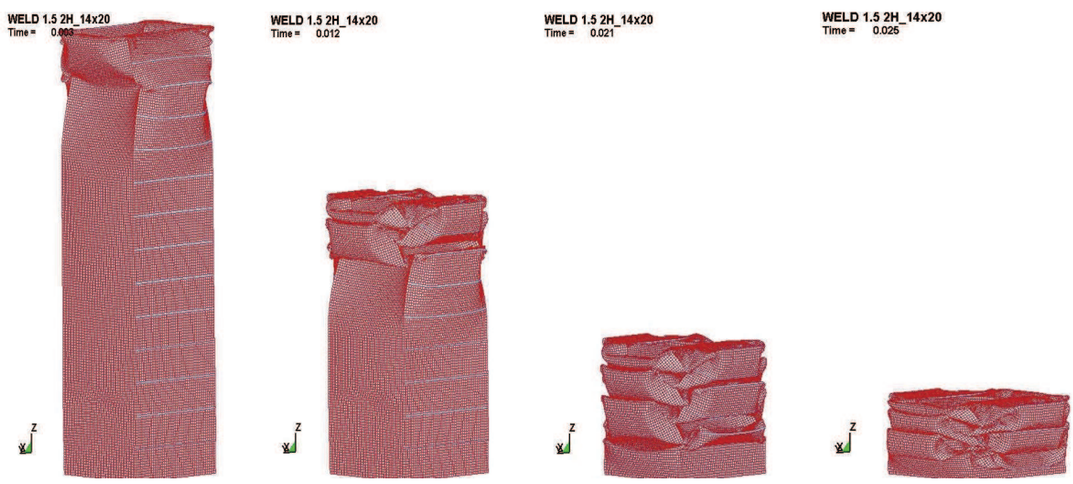

Fig. 25. Deformed shape along of the model (14x20) with 1.5mm width of the HAZ triggers.

Crash energy absorption in the axially loaded model proceeds by the folding process. The elements compressed by the axial compression at the critical load loose the stability of the equilibrium configuration of the structure. Figure 28 shows through the force-displacement curves where it is folding outward (A), contact outward (B), folding inward (C) and contact inward (D). Through the deformed shape of the model the last statement can be confirmed.
When the first fold is forming, the model reaches the maximum force capacity, which represents the first peak and is referred to as the maximum peak force. The load decrease as the first fold is being developed where the folding outward is started. After the completion of the first fold, the force reduces to the first lowest point where the contact outward happened. The further deformation causes the load to increase until the next peak is formed with the formation of the second fold. The process repeats with the folding the third, forth, and fifth folds until the kinetic energy of the striking mass has been reduced to zero, as shown in Figures 29-33.

Fig. 26. Deformed shape along of the model (4x20) with 3mm width of the four HAZ triggers.

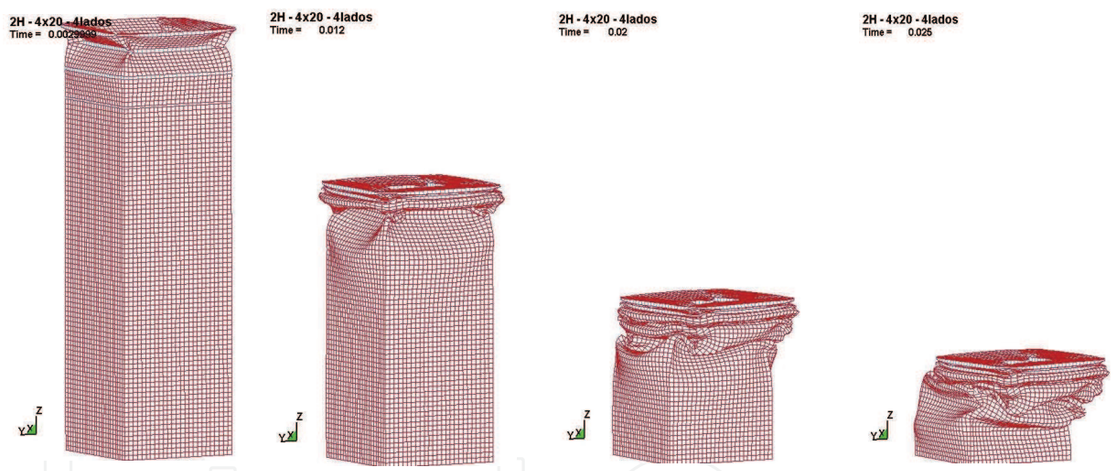

Fig. 27. Deformed shape on model with four HAZ triggers around the model with 3mm width (4sides 4x20).

Figure 29 shows the force-displacement and absorbed energy-displacement curves of the models with triggers along of the model and for the distance 40mm the results are quite different than the other ones because the first fold is forming in the top of the model but the second fold is being started at the bottom of the model. The absorption energy during the crushing process for the same displacement than the others is increasing. This model is an exception when compared to the others smart models studied here.

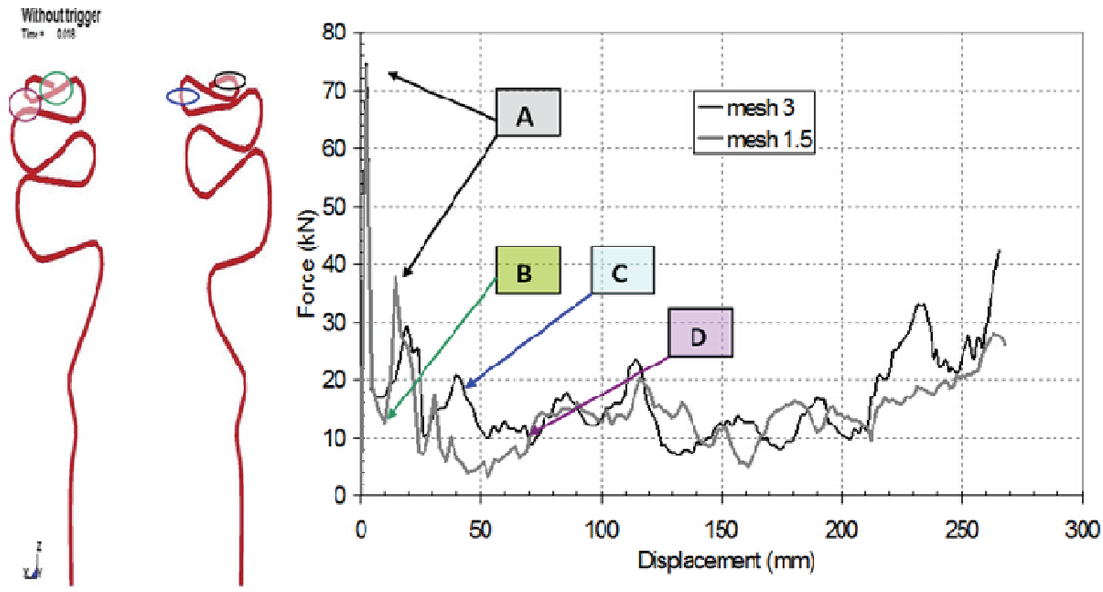

Fig. 28. Deformed shape of the model without trigger with mesh size at 3mm and force-displacement curves of the models without triggers for both mesh size.

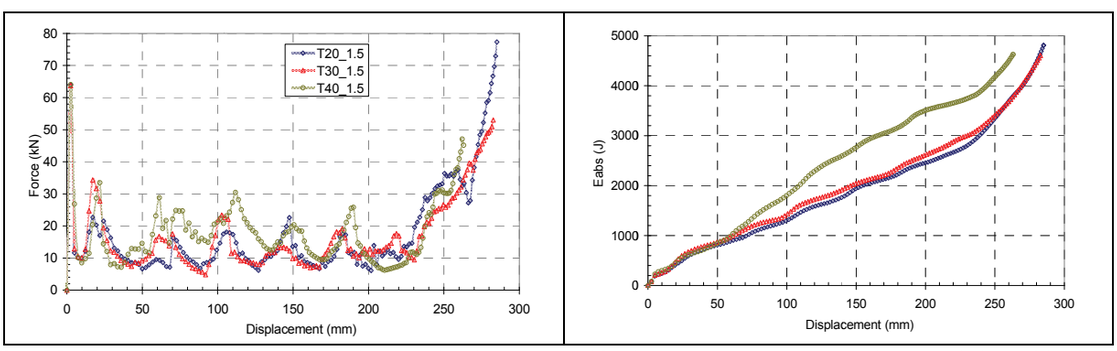

Fig. 29. Force-displacement and absorbed energy-displacement curves of the models with 1.5m wide of the HAZ triggers, on the adjacent sides at the same distance along of the model.

In the case of models without triggers, the maximum force exerted goes through a sharp maximum significantly higher than the other models, as seen in Table 3. This maximum force is effectively reduced about 14% for almost the models by the imposed HAZ triggers. The highest efficiency of energy absorption during the crushing is found in models that have four triggers in opposite sides with 1.5mm width, and in models that have four triggers around the model with 3mm width. In these cases the folds present a regular shape. This section presented research work regarding experimental results of heat-treatment of aluminium alloys with the purpose of inducing local modification of material properties. This was achieved using laser heat-treatment and in furnace tests. It was verified that it is possible to change the local hardness in a controlled way, i.e. by the copper rich precipitates dissolution effect in the sample, with a laser treatment, by changing the feed rate.

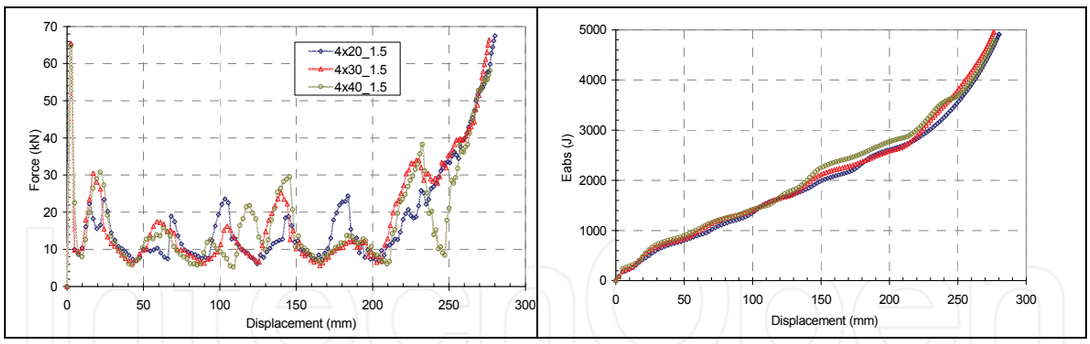

Fig. 30. Force -displacement and absorbed energy-displacement curves of the models with four HAZ triggers on the opposite sides with 1.5mm of the width.

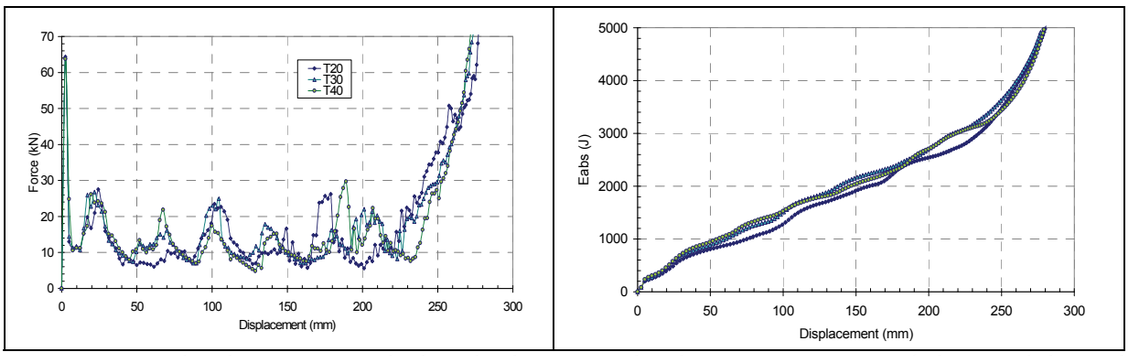

Fig. 31. Force-displacement and absorbed energy-displacement curves of the models with 3mm wide of the HAZ triggers, on the opposite sides at the same distance along of the model.

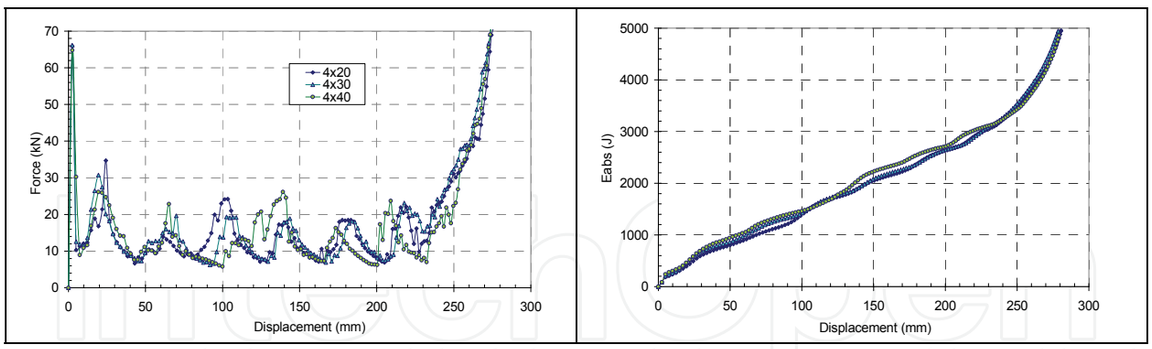

Fig. 32. Force -displacement and absorbed energy-displacement curves of the models with four HAZ triggers on the opposite sides with 3mm of the width.

Numerical simulations of crushing behaviour of aluminium tubes with local triggers obtained through heat treatment were performed. The highest efficiency of absorption energy during crushing is found in models that have four triggers in opposite sides with 1.5mm wide, and in models with four triggers around the model and 3mm width.

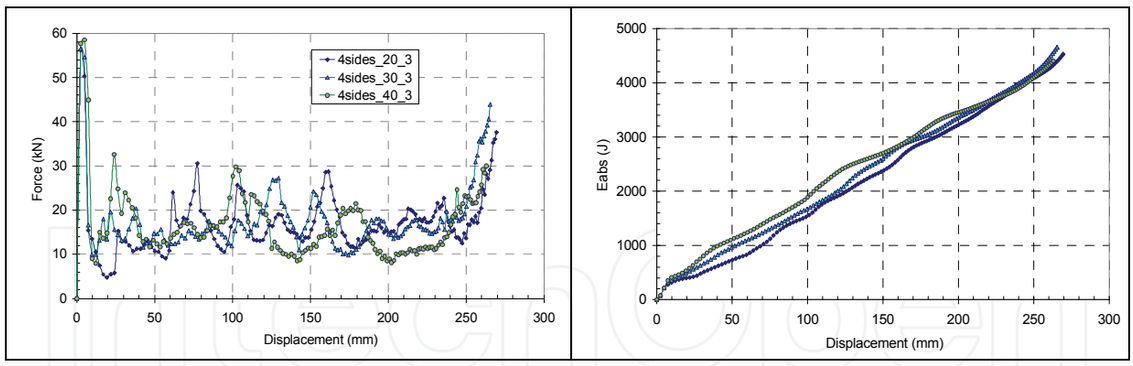

Fig. 33. Force-displacement and absorbed energy-displacement curves of the models with four HAZ around the entire model with 3mm of the width.

ITEM			Δl	E_{int}	F_{peak}	F_{med}	**Folds**
			mm	J	kN	kN	
Without trigger		mesh 3	262.0	4508	74.6	17.6	7
		mesh 1.5	268.0	4466	74.2	15.1	10
WELD 1.5	2 sides	14x20	277.3	4332	63.9	16.1	8
		9x30	277.6	4364	63.8	15.6	8
		6x40	253.6	4282	64.0	16.4	8
		4x20	274.1	4562	65.2	17.3	7
		4x30	270.5	4631	65.5	17.9	7
		4x40	273.3	4593	64.8	16.4	8
WELD 3	2 sides	14x20	275.9	4690	64.3	19.5	7
		9x30	258.3	4394	56.5	17.0	7
		6x40	259.7	4314	57.7	16.5	8
		4x20	273.4	4396	65.9	17.7	7
		4x30	271.7	4457	66.2	18.2	7
		4x40	271.5	4255	64.2	16.6	8
	4 sides	4x20	267.4	4455	56.2	16.5	10
		4x30	258.4	4394	56.4	18.0	8
		4x40	259.7	4313	58.5	16.5	5

Table 3. Numerical results

The research revealed that, by using a thermal trigger, a reduction of 15% of the initial crushing force is achievable. It is also found that this thermal trigger can not only reduce the initial maximum force but also ensure stable and uniform absorbed energy at most smart models.
The concept of using thermal modification of an aluminium alloy in localized areas for providing a larger global deformation of a part and higher energy absorption before failure appears as possible and effective in the experimental work presented and numerical simulations.

4. References

Auto/Steel Partnership, (1998). *Automotive design manual*, version 5.1, edited by American Iron and Steel Institute – Auto/Steel Partnership, 1998.

Bjørneklett, B. ; Myhr, O., (2003). Materials Design and Thermally Induced Triggers in Crash Management, *Proceedings IBEC Conference*, 2003.

Cheng, C. ; Jie, M. ; Chan, L. ; Chow, L., (2007). True stress–strain analysis on weldment of heterogeneous tailor-welded blanks—a novel approach for forming simulation, *International Journal of Mechanical Sciences*, Volume 49, Issue 2, 2007, Pages 217-229.

Gaied, S. ; Roelandt, J-M ; Pinard, F.; Schmit, F. ; Balabane, L., (2009). Experimental and numerical assessment of Tailor-Welded Blanks formability, *Journal of Materials Processing Technology*, Volume 209, Issue 1, 2009, Pages 387-395.

Geoffroy, J. ; Cambien, I. ; Jouet, A., (1993). Contribution of high strength steels to the absorption of impact energy. *La metallurgia Italiana* 1993;85(6):377–82.

Kim, H-S, (2002). New extruded multi-cell aluminium profile for maximum crash energy absorption and weight efficiency, *Thin-Walled Structures*, 40, pp. 311-327, 2002.

Kim, J. ; Kim, N. ; Huh, M., (2000). Optimum blank design of an automobile sub-frame, *Journal of Materials Processing Technology*, Volume 101, Issues 1-3, 2000, Pages 31-43.

Lee, S.; Hahn, C. ; Rhee, M. ; Ohd, J., (1999). Effect of triggering on the energy absorption capacity of axially compressed aluminum tubes, *Materials and Design*, 20, pp.31-40, 1999.

Liu, G. ; Yuan, S. ; Chu, G., (2007). FEA on deformation behavior of tailor-welded tube in hydroforming, *Journal of Materials Processing Technology*, Volumes 187-188, 2007, Pages 287-291.

Padmanabhan, R.; Oliveira, M.; Menezes, L., (2008). Deep drawing of aluminium–steel tailor-welded blanks, *Materials & Design*, Volume 29, Issue 1, 2008, Pages 154-160.

Panda, S.; Kumar, D. ; Kumar, H. ; Nath, A., (2007). Characterization of tensile properties of tailor welded IF steel sheets and their formability in stretch forming, *Journal of Materials Processing Technology*, Volume 183, Issues 2-3, 2007, Pages 321-332.

Panda, S.; Kumar, D., (2001). Improvement in formability of tailor welded blanks by application of counter pressure in biaxial stretch forming, *Journal of Materials Processing Technology*, Volume 204, Issues 1-3, 2008, Pages 70-79.

Peixinho, N., (2004). Study of viscoplasticity models for the prevision of the mechanical behaviour of high-strength steels subjected to impact, PhD thesis, University of Minho, 2004.

Peixinho, N.; Pinho, A., (2007). Study of viscoplasticity models for the impact behaviour of high-strength steels, *Journal of Computational and Nonlinear Dynamics*, Vol. 2, pp. 114-123, 2007.

Peroni, L.; Avalle, M.; Belingardi, G., (2009). Comparison of the energy absorption capability of crash boxes assembled by spot-weld and continuous joining techniques, *International Journal of Impact Engineering*, 36 (2009) 498–511.

Qiu, X.; Chen, W., (2007). The study on numerical simulation of the laser tailor welded blanks stamping, *Journal of Materials Processing Technology*, Volumes 187-188, 2007, Pages 128-131.

Radlmayr, K-M.; Ponschab, H. ; Stiaszny, P.; Till, E., (1993). Comparative behaviour of safety structures from soft and higher-tensile qualities as well as aluminium alloys in crashes. In: *Proceedings to the twenty-sixth ISATA conference on road and vehicle safety*. Aachen (Germany); 1993. Paper 93SF061.

Sheng, Z., (2008). Formability of tailor-welded strips and progressive forming test, *Journal of Materials Processing Technology*, Volume 205, Issues 1-3, 2008, Pages 81-88.

Laser Welding

Edited by Xiaodong Na, Stone

ISBN 978-953-307-129-9
Hard cover, 240 pages
Publisher Sciyo
Published online 17, August, 2010
Published in print edition August, 2010

This book is entitled to laser welding processes. The objective is to introduce relatively established methodologies and techniques which have been studied, developed and applied either in industries or researches. State-of-the art developments aimed at improving or next generation technologies will be presented covering topics such as monitoring, modelling, control, and industrial application. This book is to provide effective solutions to various applications for field engineers and researchers who are interested in laser material processing.

How to reference

In order to correctly reference this scholarly work, feel free to copy and paste the following:

Nuno Peixinho (2010). Laser Welding Application in Crashworthiness Parts, Laser Welding, Xiaodong Na, Stone (Ed.), ISBN: 978-953-307-129-9, InTech, Available from: http://www.intechopen.com/books/laser-welding/laser-welding-application-in-crashworthiness-parts

INTECH
open science | open minds

InTech Europe
University Campus STeP Ri
Slavka Krautzeka 83/A
51000 Rijeka, Croatia
Phone: +385 (51) 770 447
Fax: +385 (51) 686 166
www.intechopen.com

InTech China
Unit 405, Office Block, Hotel Equatorial Shanghai
No.65, Yan An Road (West), Shanghai, 200040, China
中国上海市延安西路65号上海国际贵都大饭店办公楼405单元
Phone: +86-21-62489820
Fax: +86-21-62489821

IntechOpen